

# Characterization of passivity and pitting corrosion of 3003 aluminum alloy in ethylene glycol–water solutions

Y. Liu · Y. F. Cheng

Received: 5 February 2010/Accepted: 18 September 2010/Published online: 22 September 2010  
© Springer Science+Business Media B.V. 2010

**Abstract** In this work, the passivity and pitting corrosion behavior of 3003 aluminum (Al) alloy in ethylene glycol–water solutions was investigated using various electrochemical measurements, Mott–Schottky analysis and surface analysis techniques. Results demonstrate that the passive film formed on Al alloy contains both Al oxide and Al alcohol, showing an *n*-type semiconductor in nature. There is an enhanced corrosion resistance of the Al-alcohol film, which is resistant to adsorption of chloride ions. The pitting corrosion of 3003 Al alloy occurs in the solutions containing a low concentration of ethylene glycol only, where the formed film is dominated by Al oxide. Chloride ions attack and replace the oxygen vacancies in the film, resulting in a local detachment of the film from the Al alloy. A galvanic effect exists between Al alloy substrate and the adjacent second phase particles. Pits form when Al alloy substrate is dissolved away and the second phase particles drop off from the substrate.

**Keywords** Passivity · Pitting corrosion · Aluminum alloy · Ethylene glycol

## 1 Introduction

Aluminum (Al) alloys, due to their favorable strength-to-weight property, high thermal conductivity, and excellent formability, have been widely used in automobile heat exchange system, replacing traditional materials like stainless steels and copper alloys [1, 2]. However, Al alloys

are prone to experience corrosion and pitting corrosion in automotive cooling system, which generally contains ethylene glycol as anti-freezer [3–5].

It has been acknowledged [6–9] that the corrosion resistance of Al alloys depends on the formation of a layer of passive film on their surface in the environments. A significant number of works have been performed to characterize the passive films formed under various conditions [10–18]. For example, Bockris and coworkers [10, 11] found a two-layer structure of passive film formed on Al alloy in sodium borate solution. While the outer layer is a mixture of  $\text{Al}_2\text{O}_3$  and  $\text{Al}(\text{OH})_3$ , the inner layer is composed of  $\text{Al}_2\text{O}_3$  and  $\text{AlOOH}$ . Furthermore, the structure of the passive film on Al alloy is dependent on the forming solution. It was found [6] that passive film formed in a borate and tartaric acid solution is thin, dense, and coherent, whereas that formed in sulfuric and phosphoric acids shows a thick, porous, and crystalline layer. With respects to the semiconducting property of the passive film formed on Al alloys, there have existed controversial results. Fernandes et al. [12] reported that the passive film formed on 2024 Al alloy in a sulphuric–boric bath shows an *n*-type semiconducting behavior, while Levine et al. [13] determined that the passive film on 2024 Al alloy is a *p*-type semiconductor. Liu et al. [19] demonstrated that passive films formed on 3003 Al alloy in air and in  $\text{Na}_2\text{SO}_4$  solutions in the absence and presence of chloride ions show an *n*-type semiconductor in nature.

To date, research in passivity and corrosion of Al alloy in automotive coolant, i.e., ethylene glycol–water solutions, has been in its infancy. Cheng's group [20–25] studied systematically the flow-assisted corrosion and erosion-corrosion of 3003 Al alloy in aqueous ethylene glycol solutions. It was proposed that the passive film formed on the Al alloy contains primarily Al-alcohol film,

Y. Liu · Y. F. Cheng (✉)  
Department of Mechanical and Manufacturing Engineering,  
University of Calgary, Calgary, AB T2N 1N4, Canada  
e-mail: fcheng@ucalgary.ca

which is resistant to the attack by chloride ions ( $\text{Cl}^-$ ). In particular, Zhang et al. [23] proposed an electrochemical reaction mechanism to illustrate the formation of the Al-alcohol film. They used energy-dispersive X-ray analysis (EDAX) to detect the presence of a significant amount of carbon in the film, which was assumed to be an indicator of the formation of an Al-alcohol film. Moreover, the metal–alcohol film was also found to form on other metals, such as steels [26–28]. However, a direct evidence for the formation of an Al-alcohol film in the ethylene glycol–water solution has so far been lacking. Furthermore, an exact mechanism illustrating the occurrence of pitting corrosion on Al alloy in ethylene glycol solutions has been remained unknown.

In this work, the passivity and pitting corrosion behavior of 3003 Al alloy (AA3003) in ethylene glycol–water solutions was investigated using various electrochemical measurement techniques, including cyclic polarization, linear polarization resistance, and electrochemical impedance spectroscopy (EIS) measurements. The passive film was characterized by Mott–Schottky analysis, scanning electron microscopy (SEM), and X-ray photoelectron spectroscopy (XPS). The occurrence of pitting corrosion was discussed mechanistically.

## 2 Experimental

### 2.1 Electrode and solution

Test specimens were cut from a round bar of AA3003 supplied by Dana Canada Corporation, with the chemical composition (wt%): Cu 0.20, Fe 0.70, Si 0.60, Mn 1.50, Mg 0.05, Cr 0.05, Zn 0.10, Ti 0.05, and Al balance. Specimens were machined and embedded in an epoxy resin manufactured by LECO, leaving a square working area of 1 cm<sup>2</sup>. The working surface of the specimen was ground with emery papers up to 1200 grit and cleaned by deionized water.

The test solutions were ethylene glycol–water solutions with addition of 100 ppm  $\text{Cl}^-$  (weight/weight) in the form of NaCl, simulating the automotive coolant. Table 1 shows the various test solutions and their properties, including solution pH, dissolved oxygen concentration, conductivity, and absolute viscosity. All solutions were made from analytical grade chemicals and deionized water with a resistivity of 18 MΩ cm.

### 2.2 Electrochemical measurements

Electrochemical measurements were conducted through a three-electrode cell, with AA3003 as working electrode

**Table 1** Some parameters of 0, 50, 70, and 100% (v/v) ethylene glycol–water solutions containing 100 ppm  $\text{Cl}^-$

Glycol concentration (v/v, %)	Dissolved oxygen concentration (mg L <sup>-1</sup> )	pH	Conductivity ( $\mu\text{S cm}^{-1}$ )	Absolute viscosity (mPa s)
0	4.21	6.20	820.6	1.0
50	2.53	6.97	258.5	2.15
70	1.95	7.18	149.8	3.85
100	1.57	7.48	41.36	23

(WE), a saturated calomel electrode (SCE) as reference electrode (RE) and a Pt wire as counter electrode (CE), using a Solartron 1280C electrochemical system. The IR drop compensation mode of the instrument was set at ON with an input value around 6,000 Ω, which was estimated through the EIS measurement.

Prior to electrochemical measurement, the Al alloy WE was immersed in the solution at least 1 h until its corrosion potential ( $E_{\text{corr}}$ ) reached a steady-state value. Cyclic polarization scan was performed at a positive direction with a potential sweep rate of 1 mV s<sup>-1</sup>. The scan direction was reversed when the anodic current density reached 100  $\mu\text{A cm}^{-2}$ . Each measurement was performed three times to ensure the reproducibility of the result. The values of polarization resistance, corrosion current density, and corrosion potential were fitted through a PowerCORR analytical software.

The space-charge layer capacitance measurement was conducted with an applied AC disturbance signal of 10 mV at a fixed frequency of 1,000 Hz. The potential dependence of the space-charge layer capacitance ( $C_{\text{sc}}$ ) is expressed by Mott–Schottky relationship [29]:

For an *n*-type semiconductor:

$$\frac{1}{C_{\text{SC}}^2} = \frac{2}{e\epsilon_r\epsilon_0 N_D} (E - \phi_{\text{fb}} - \frac{\kappa T}{e}) \quad (1)$$

For a *p*-type semiconductor:

$$\frac{1}{C_{\text{SC}}^2} = -\frac{2}{e\epsilon_r\epsilon_0 N_A} (E - \phi_{\text{fb}} - \frac{\kappa T}{e}) \quad (2)$$

where  $e$  is electron charge ( $1.6 \times 10^{-19}$  C),  $\epsilon_r$  is dielectric constant of Al oxide, taken as 10 [30],  $\epsilon_0$  is the vacuum permittivity ( $8.85 \times 10^{-14}$  F cm<sup>-1</sup>),  $N_D$  is the donor density,  $N_A$  is the acceptor density,  $E$  is the applied potential,  $\phi_{\text{fb}}$  is flat-band potential,  $\kappa$  is Boltzmann constant ( $1.38 \times 10^{-23}$  J K<sup>-1</sup>), and  $T$  is absolute temperature.  $N_D$  and  $N_A$  can be determined from the slope of the linear relationship between  $C_{\text{sc}}^{-2}$  and  $E$ .

In measurement of the potential of zero charge (PZC) of the Al alloy WE, a frequency of 18 Hz was applied. In both  $C_{\text{sc}}$  and PZC measurements, a potentiodynamic scan was

synchronously applied on WE, with a potential scanning step of 20 mV.

All the tests were performed at ambient temperature ( $\sim 22^\circ\text{C}$ ) and open to air.

### 2.3 Surface characterization

The AA3003 specimens were immersed in 50, 70, and 100% (v/v) ethylene glycol–water solutions for 3 days, and were then removed from the solutions, rinsed with deionized water, dried with cold air, and sent for surface analysis. The morphology of the electrode was observed using a Philips XL30 SEM.

The XPS characterization was carried out by using a VG ESCALAB-MKII XPS equipped with a dual anode X-ray source ( $\text{MgK}\alpha = 1253.6\text{ eV}$ ,  $\text{AlK}\alpha = 1486.6\text{ eV}$ ) with a pass energy of 50 eV. The spectra were recorded in both an overall range of 0–1100 eV and the specific regions of  $\text{Al}^{2p1}$  (65–85 eV),  $\text{C}^{1s}$  (275–295 eV), and  $\text{O}^{1s}$  (522–542 eV). Standard  $\text{C}^{1s}$  sample was added as a calibrator. The standard chemical bonding energy was cited as a Ref. [31].

## 3 Results

### 3.1 Polarization measurements

Figure 1 shows the anodic cyclic polarization curves measured on AA3003 electrode in 0, 50, 70, and 100% (v/v) ethylene glycol–water solutions containing 100 ppm

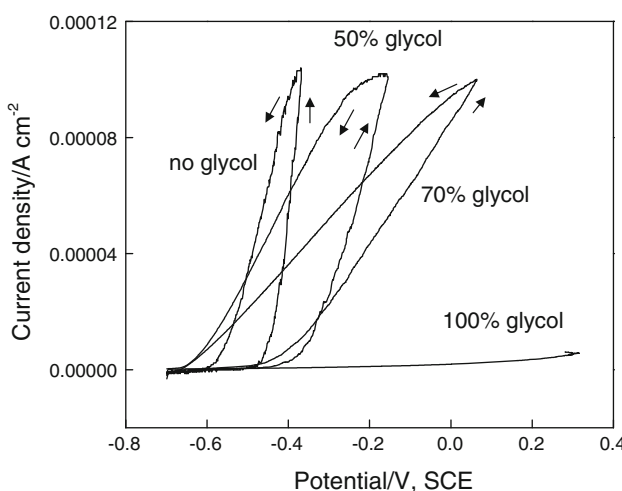


**Fig. 1** Anodic cyclic polarization curves measured on AA3003 electrode in 0, 50, 70, and 100% (v/v) ethylene glycol–water solutions containing 100 ppm  $\text{Cl}^-$ , where the solid arrows indicate the potential scanning direction

$\text{Cl}^-$ . It is seen that Al alloy would be passivated in all solutions. The anodic current density measured in the ethylene glycol-free solution increased rapidly at pitting potential ( $E_{\text{pit}}$ ), which was defined as the potential where the anodic current density exceeds a randomly determined threshold of  $2\text{ }\mu\text{A cm}^{-2}$ , of approximately  $-0.48\text{ V (SCE)}$ . When the solution contained 50 and 70% (v/v) ethylene glycol, the  $E_{\text{pit}}$  was shifted positively to  $-0.4\text{ V (SCE)}$ . In 100% ethylene glycol, the current density remained quite low over the whole potential range, and the pre-set reversing threshold current density ( $100\text{ }\mu\text{A cm}^{-2}$ ) was never reached. Except the polarization curve measured in 100% ethylene glycol, the other curves were featured with a positive hysteresis loop during reverse potential scanning. Moreover, the current density rising rate after  $E_{\text{pit}}$  decreased with the increase of the ethylene glycol concentration in the solution.

Figure 2 shows the linear polarization resistance of the AA3003 electrode measured in 0, 50, 70, and 100% (v/v) ethylene glycol–water solutions containing 100 ppm  $\text{Cl}^-$ . Although the measured results did not follow a strict linear relationship between  $E$  and  $i$ , a qualitative analysis was performed to determine the effect of the concentration of ethylene glycol in the solution on corrosion of AA3003. According to Stern and Geary model [32, 33], the polarization resistance ( $R_p$ ) can be obtained from the fitting slope ( $dE/di$ ) of the linear relationship between potential and current density:

$$R_p = \left[ \frac{\Delta E}{\Delta i} \right]_{\Delta E \rightarrow 0} \quad (3)$$

The corrosion current density ( $i_{\text{corr}}$ ) was calculated by:

$$i_{\text{corr}} = \frac{B}{R_p} \quad (4)$$

where  $B$  is a proportionality constant which is usually taken as 26 mV [9].

The fitting values of  $R_p$ ,  $i_{\text{corr}}$ , and  $E_{\text{corr}}$  are listed in Table 2. It is seen that, with the increase of the ethylene glycol concentration, the polarization resistance increased, and the corrosion current density decreased.

### 3.2 Capacitance measurements and Mott–Schottky analysis

Figure 3 shows the Mott–Schottky curves of AA3003 electrode in 0, 50, 70, and 100% (v/v) ethylene glycol–water solutions containing 100 ppm  $\text{Cl}^-$ . It is seen that a positive slope was observed in all Mott–Schottky plots, indicating that passive films formed in all solutions behaved like an  $n$ -type semiconductor. The donor densities in the passive films formed in 0, 50, 70, and 100% (v/v)

**Fig. 2** Linear polarization resistance of AA3003 electrode measured in 0, 50, 70, and 100% (v/v) ethylene glycol–water solutions containing 100 ppm  $\text{Cl}^-$

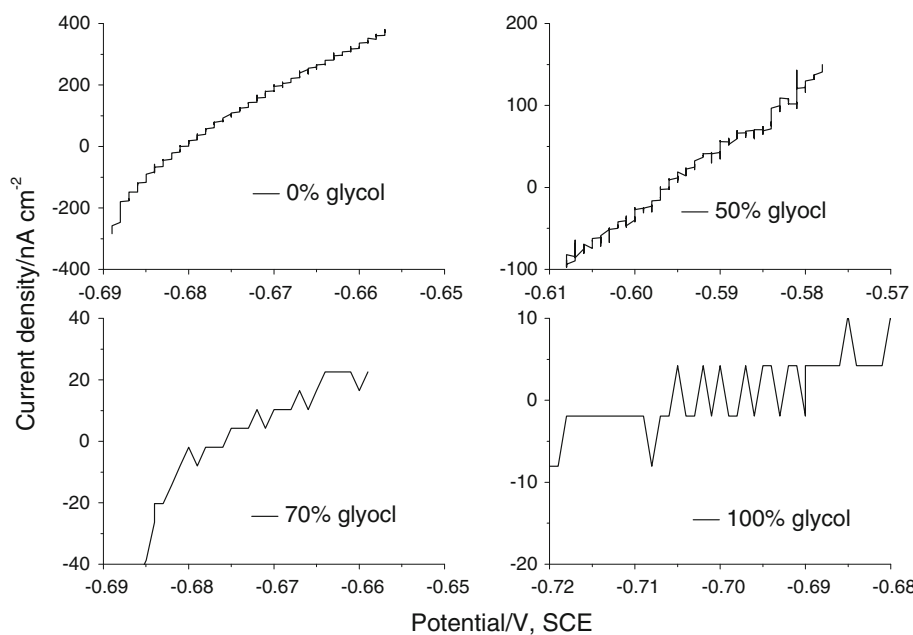


**Table 2** Electrochemical parameters fitted from the linear polarization resistance measurements for AA3003 electrode in 0, 50, 70, and 100% (v/v) ethylene glycol–water solutions containing 100 ppm  $\text{Cl}^-$

Glycol concentration (v/v, %)	$R_p$ ( $\times 10^5$ , $\Omega \text{ cm}^2$ )	$i_{\text{corr}}$ ( $\text{nA cm}^{-2}$ )	$E_{\text{corr}}$ (V, SCE)
0	0.497	525	-0.68
50	1.25	208	-0.60
70	6.94	37.6	-0.67
100	34.8	7.51	-0.70

ethylene glycol–water solutions were  $3.2 \times 10^{28}$ ,  $6.1 \times 10^{27}$ ,  $4.8 \times 10^{27}$ , and  $5.1 \times 10^{26} \text{ m}^{-3}$ , respectively. Apparently, the donor density decreased with the increasing ethylene glycol concentration.

### 3.3 PZC measurements

Figure 4 shows the Al alloy electrode/solution interfacial capacitances measured in 50, 70, and 100% (v/v) ethylene glycol–water solutions with 100 ppm  $\text{Cl}^-$ , respectively, as a function of applied potential. It is seen that there was a common feature for all curves, i.e., a minimum of the interfacial capacitance that was considered as PZC of the Al alloy electrode was observed. The values of PZC measured in the solutions and the differences between PZC and  $E_{\text{corr}}$  ( $\Delta E = E_{\text{corr}} - \text{PZC}$ ) are listed in Table 3, where the values of  $E_{\text{corr}}$  were taken from Table 2. It is seen that there was a more negative PZC than  $E_{\text{corr}}$  for all electrodes. Moreover, an increase of ethylene glycol concentration in the solution would decrease  $\Delta E$ .

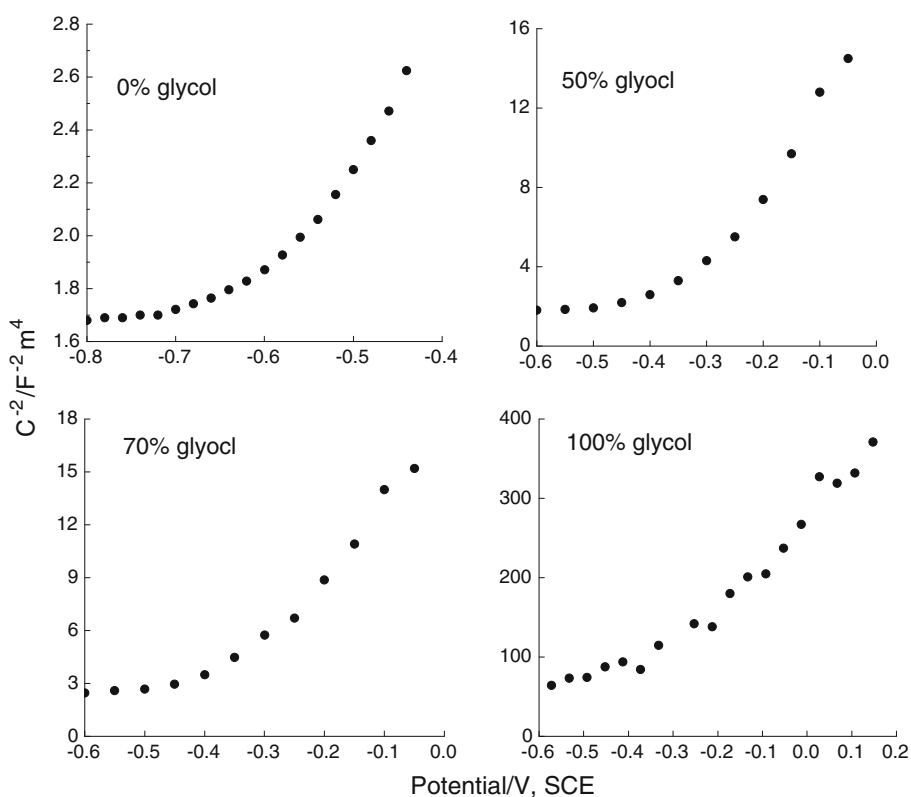
### 3.4 Surface morphology observation

Figure 5 shows the SEM views of the surface morphology of AA3003 specimens after 3 days of immersion in 50, 70, and 100% (v/v) ethylene glycol–water solutions containing 1000 ppm  $\text{Cl}^-$ , where the  $\text{Cl}^-$  concentration was raised by 10 times compared with previous tests in order to test the pitting susceptibility of the Al alloy. A number of second phase particles shaped of stretched ellipses were observed in the Al alloy substrate. The specimen immersed in 50% (v/v) ethylene glycol–water solution suffered from extensive pitting corrosion, and the initiation of pits was associated with the local dissolution of Al alloy substrate around the second phase particles. However, pits were not observed on the specimens immersed in 70 and 100% (v/v) ethylene glycol–water solutions.

### 3.5 Composition characterization of the passive film

Figure 6a shows an overview of XPS spectrum obtained on AA3003 electrode self-passivated in 50% (v/v) ethylene glycol–water solution containing 100 ppm  $\text{Cl}^-$  for 3 days. It is seen that the peaks of  $\text{C}^{1s}$  and  $\text{O}^{1s}$  were distinguishable in the spectrum. The Al peak appeared clearly in the specific scan (Fig. 6b). Moreover, it was found that the  $\text{C}^{1s}$  spectrum (Fig. 6d) showed a slight positive deflection from the standard chemical bonding energy of  $\text{C}^{1s}$  (284.6 eV), indicating that the chemical valence of carbon in passive film is more positive than carbon element. The deflection was clearly presented as an inverse  $\text{C}^{1s}$  peak in Fig. 6e, which was deducted from the standard carbon peak by the positive  $\text{C}^{1s}$  peak in the film.

**Fig. 3** Mott–Schottky curves of AA3003 electrode in 0, 50, 70, and 100% (v/v) ethylene glycol–water solutions containing 100 ppm  $\text{Cl}^-$

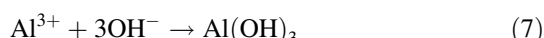
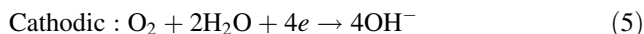


## 4 Discussion

### 4.1 Passivity of AA3003 in ethylene glycol–water solutions

Generally, the passive film formed on Al alloys in aqueous solutions contains primarily aluminum oxide [10, 12, 34], which behaves like an *n*-type semiconductor [19, 29]. This work also demonstrates that passive films formed on AA3003 in ethylene glycol–water solutions show an *n*-type semiconductor in nature, as indicated by the positive slope in Mott–Schottky plots in Fig. 3.

In a glycol-free aqueous solution, the cathodic and anodic reactions during corrosion of Al alloy are [32]:



Upon the addition of ethylene glycol in the solution, ethylene glycol would be reduced and an Al-alcohol film is formed:



The XPS results (Fig. 6) reveal that carbon contained in the film formed on the Al alloy surface has a positive valence, which is resulted from the presence of C–O bond in the

film. The existence of C–O bonds provides direct evidence that the Al-alcohol film is formed on Al alloy in ethylene glycol–water solutions.

### 4.2 Pitting corrosion of AA3003 in ethylene glycol–water solutions

As discussed, a layer of Al-alcohol film is formed on the Al alloy surface, enhancing the corrosion resistance of Al alloy. The anodic cyclic polarization measurements (Fig. 1) show that, with the increase of the ethylene glycol concentration, the anodic current density decreases. In particular, in 100% ethylene glycol, there is a quite low current density even when the potential is as positive as 0.2 V (SCE). The linear polarization resistance measurements (Fig. 2; Table 2) also confirm the enhanced corrosion resistance of Al alloy in the presence of ethylene glycol.

Furthermore, the film formed on the Al alloy electrode surface, containing both Al oxide and Al alcohol, shows an *n*-type semiconducting property (Fig. 3). According to point defect model (PDM) [34, 35], for an *n*-type semiconductor, the primary electron donors are oxygen vacancies, which could be replaced by chloride ions to generate cation vacancies at the film/solution interface. The cation vacancies transport towards the metal/film interface to produce cation vacancy condensate, resulting in a local detachment of the film and pitting. Therefore, the

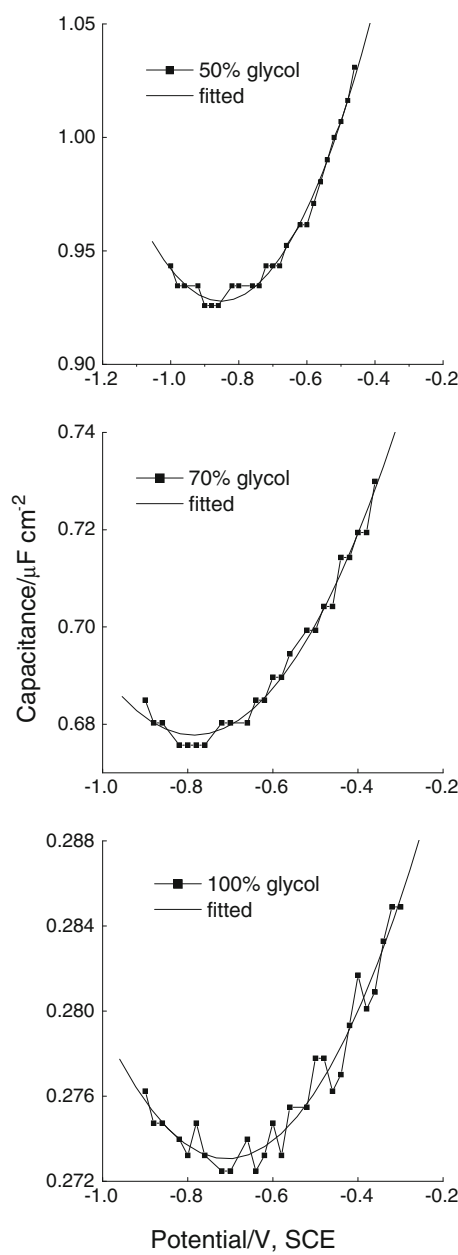


**Fig. 4** The Al alloy electrode/solution interfacial capacitance measured in 50, 70, and 100% (v/v) ethylene glycol–water solutions with 100 ppm  $\text{Cl}^-$ , respectively, as a function of applied potential

**Table 3** Potential of zero charge and the difference between  $E_{\text{corr}}$  and PZC for AA3003 electrode in 50, 70, and 100% (v/v) ethylene glycol–water solutions containing 100 ppm  $\text{Cl}^-$

Glycol concentration (v/v %)	PZC (V, SCE)	$E_{\text{corr}}$ (V, SCE)	$\Delta E = E_{\text{corr}} - \text{PZC}$ (V)
50	-0.85	-0.60	0.25
70	-0.78	-0.67	0.11
100	-0.72	-0.70	0.02

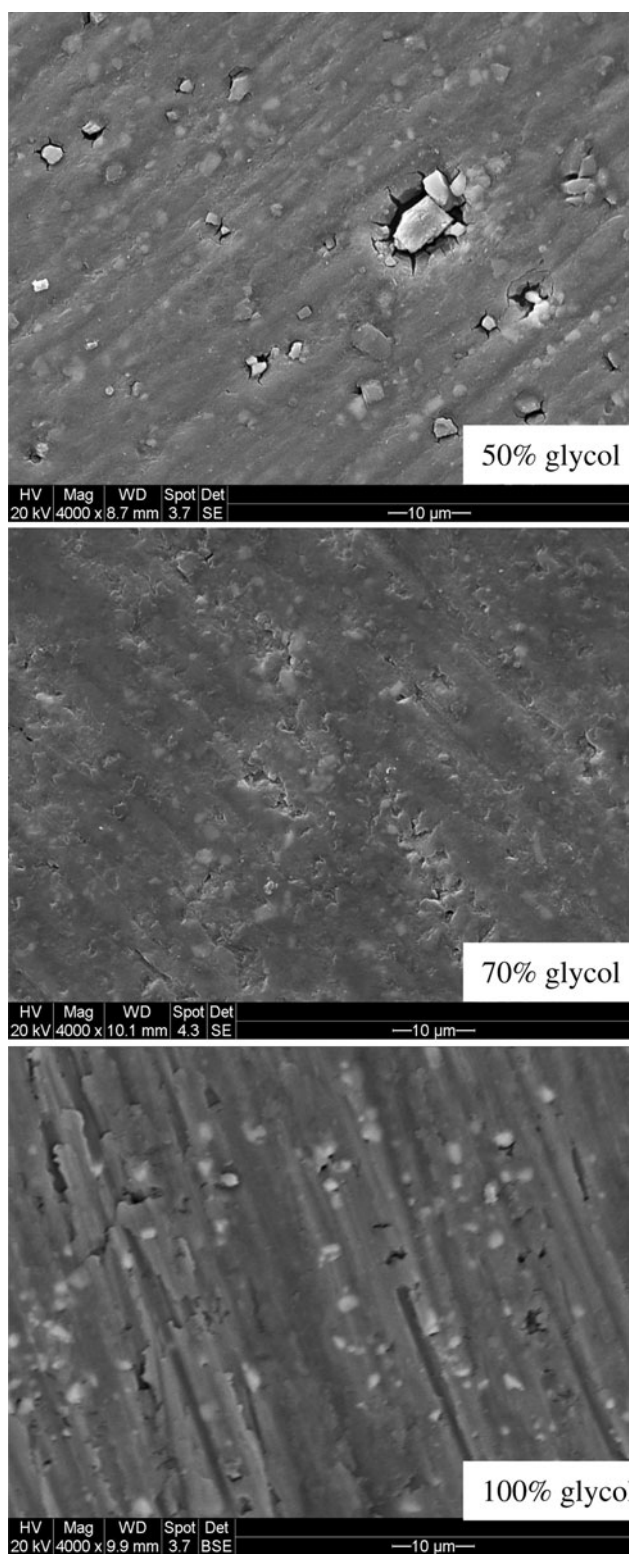
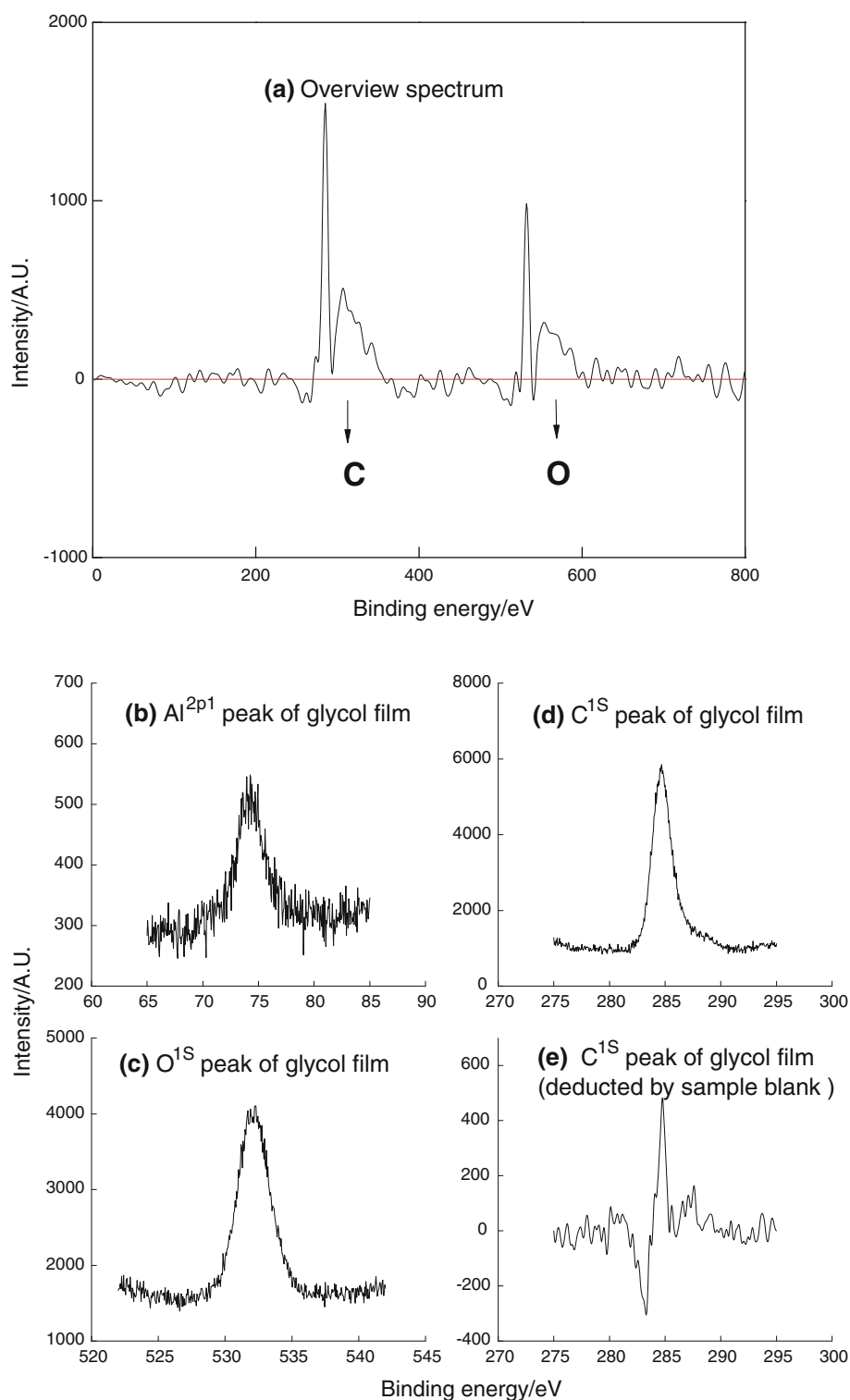


**Fig. 5** SEM views of the surface morphology of AA3003 specimens after 3 days of immersion in 50, 70, and 100% (v/v) ethylene glycol–water solutions containing 1000 ppm  $\text{Cl}^-$

**Fig. 6** XPS spectra of AA3003 electrode after 3 days of immersion in 50% (v/v) ethylene glycol–water solution containing 100 ppm  $\text{Cl}^-$   
**a** overview spectrum; **b**  $\text{Al}^{2\text{p}1}$  peak; **c**  $\text{O}^{1\text{s}}$  peak; **d**  $\text{C}^{1\text{s}}$  peak;  
**e**  $\text{C}^{1\text{s}}$  peak deducted by sample blank



susceptibility of a passive film to pitting depends on its donor density. This work establishes that the donor density of the passive film decreases with the increase of ethylene glycol in the solution, indicating that the addition of ethylene glycol would affect the pitting susceptibility of the

passivated Al alloy by altering the composition and electronic structure of the passive film.

The PZC measurement is usually used to “visualize” the surface adsorption phenomenon on an electrode [19]. With the increase of ethylene glycol concentration in the

solution, the difference between  $E_{corr}$  and PZC decreases, as seen in Fig. 4, indicating a decreasing adsorption of ionic species, specifically chloride ions, on the electrode surface. Furthermore, the thickness of the space-charge layer in passive film increases and the space-charge layer capacitance decreases with the increase of the ethylene glycol concentration, which is associated with an enhanced stability of the passive film. Therefore, with the increase of ethylene glycol concentration in the solution, it is expected that the proportion of Al-alcohol film increases, resulting in a decrease of the proportion of Al oxide in the film, and thus the amount of oxygen vacancies in the passive film. As a consequence, the sites available for the chloride ion adsorption decreases, so is the pitting susceptibility.

In the previous work [36], it was established that a galvanic effect exists between the Mn-enriched second phase particles and the adjacent Al alloy substrate, where second phase particles serve as the cathode and Al alloy as the anode. Occurrence of pitting corrosion of Al alloy is resulted from the local dissolution of the Al alloy substrate around the second phase particles. In this work it is observed that the corrosion pits are always associated with corrosion of the adjacent Al alloy substrate (Fig. 5a). When a sufficient amount of Al alloy is dissolved away, the second phase particles drop off from the substrate, forming corrosion pits.

To summarize, the pitting corrosion of AA3003 in ethylene glycol–water solutions occurs in solutions containing a low concentration of ethylene glycol only, where the formed film is dominated by Al oxide. Upon attack of chloride ions to take place of oxygen vacancies, the film is broken and detached from the Al alloy locally around the second phase particles. A galvanic effect occurs between the Al alloy substrate and the adjacent second phase particles, resulting preferential dissolution of Al alloy and the drop of the particles off the Al alloy substrate. With the increase of the amount of ethylene glycol in the solution, the film becomes Al-alcohol dominant, which inhibits the adsorption of chloride ions and enhances the stability of the film. Thus, pitting would not occur in the solutions with a sufficiently high ethylene glycol concentration.

## 5 Conclusions

The passive film formed on AA3003 in ethylene glycol–water solutions contains both Al oxide and Al alcohol, and the proportion of the two films depends on the amount of ethylene glycol contained in the solution. The formed film shows an *n*-type semiconductor in nature.

With the increase of ethylene glycol in the solution, the proportion of the Al-alcohol film increases and that of Al oxide decreases. Consequently, the amount of oxygen

vacancies in the film decreases, inhibiting the adsorption of chloride ions on the film. Thus, the pitting susceptibility of the passivated Al alloy decreases with the increasing ethylene glycol concentration.

The pitting corrosion of AA3003 occurs in solutions containing a low concentration of ethylene glycol only, where the formed film is dominated by Al oxide. Upon attack of chloride ions to take place of oxygen vacancies, the film is broken and detached from the Al alloy locally around the second phase particles. A galvanic effect occurs between the Al alloy substrate and the adjacent second phase particles, resulting preferential dissolution of Al alloy and the drop of the particles off the Al alloy substrate.

**Acknowledgments** This work was supported by Canada Research Chairs Program, Natural Science and Engineering Research Council of Canada (NSERC), and Dana Canada Corporation. The XPS tests were conducted by Dr. C.F. Dong at the University of Science and Technology Beijing.

## References

- Davies G (2003) Materials for automobile bodies. Butterworth-Heinemann, Oxford, UK
- Miller WS, Zhuang L, Bottema J, Wittebrood AJ, De Smet P, Haszler A, Vieregge A (2000) Mater Sci Eng A 280:37
- Institution of Mechanical Engineers (1976) Corrosion of motor vehicles. Mechanical Engineering Publications Limited, London, UK
- Babolian R (1981) Automotive corrosion by deicing salts. National Association of Corrosion Engineers, Houston, USA
- Wong D, Swette L (1979) J Electrochem Soc 126:11
- Szklarska-Smialowska Z (1999) Corros Sci 41:1743
- Frankel GS (1998) J Electrochem Soc 145:2186
- Fontana MG (1990) Corrosion engineering. McGraw-Hill, CA, USA
- Kelly RG, Scully JR, Shoesmith DW, Buchheit RG (2003) Electrochemical techniques in corrosion science and engineering. Marcel Dekker, Inc, NY, USA
- Bockris JOM, Kang Y (1997) J Solid State Electrochem 1:17
- Bockris JOM, Minevski LV (1993) J Electroanal Chem 349:375
- Fernandes JCS, Picciuchi R, Da Cunha Belo M, Silva TM, Ferreira MGS, Fonseca ITE (2004) Electrochim Acta 49:4701
- Levine KL, Tallman DE, Bierwagen GP (2008) J Mater Process Technol 199:321
- Mansfeld F (1990) Electrochim Acta 35:1533
- Mansfeld F, Shih H (1988) J Electrochem Soc 135:1171
- Lee WJ, Pyun SI (1999) Electrochim Acta 44:4041
- Martin FJ, Cheek GT, O'Grady WE, Natishan PM (2005) Corros Sci 47:3187
- Wall FD, Martinez MA, Missett NA, Copeland RG, Kilgo AC (2005) Corros Sci 47:17
- Liu Y, Meng GZ, Cheng YF (2009) Electrochim Acta 54:4155
- Niu L, Cheng YF (2007) J Mater Sci 42:8613
- Niu L, Cheng YF (2008) Wear 265:367
- Zhang GA, Xu LY, Cheng YF (2009) Corros Sci 51:283
- Zhang GA, Xu LY, Cheng YF (2008) Electrochim Acta 53:8245
- Xu LY, Cheng YF (2008) Corros Sci 50:2094
- Xu LY, Cheng YF (2009) Corros Sci 51:2330
- Faidi SE, Jones G, Scantlebury JD (1987) Electrochim Acta 32:947

27. Guilminot E, Dalard F, Degrigny C (2002) Corros Sci 44:2199
28. Cheng YF (2005) Bull Electrochem 21:503
29. Morrison SR (1980) Electrochemistry at semiconductor and oxidized metal electrodes. Plenum Press, New York, USA
30. Dean MH, Stimming U (1989) Corros Sci 29:199
31. Wagner CD, Riggs WM, Davis LE, Moulder JF, Mullenberg GE (1979) Handbook of X-ray photoelectron spectroscopy. Perkin-Elmer Corp, Eden Prairie, USA
32. Stern M, Geary AL (1957) J Electrochem Soc 104:56
33. Stern M, Geary AL (1958) J Electrochem Soc 105:638
34. Macdonald DD (1992) J Electrochem Soc 139:3434
35. Macdonald DD (2006) J Electrochem Soc 153:B213
36. Liu Y, Cheng YF (2009) Mater Corros. doi:[10.1002/maco.200905308](https://doi.org/10.1002/maco.200905308)